

# A Probabilistic Forecast-Driven Strategy for a Risk-Aware Participation in the Capacity Firming Market

Jonathan Dumas, Colin Cointe, Antoine Wehenkel, Antonio Sutera, Xavier Fettweis, and Bertrand Cornélusse

**Abstract**—This paper addresses the energy management of a grid-connected renewable generation plant coupled with a battery energy storage device in the capacity firming market, designed to promote renewable power generation facilities in small non-interconnected grids. The core contribution is to propose a probabilistic forecast-driven strategy, modeled as a min-max-min robust optimization problem with recourse, and solved using a *Benders-dual cutting plane algorithm* in a tractable manner. The convergence is improved by building an initial set of cuts. In addition, a dynamic risk-averse parameters selection strategy based on the quantile forecasts distribution is proposed. A secondary contribution is to use a recently developed deep learning model known as normalizing flows to generate quantile forecasts of renewable generation for the robust optimization problem. This technique provides a general mechanism for defining expressive probability distributions, only requiring the specification of a base distribution and a series of bijective transformations. Overall, the robust approach improves the results over a deterministic approach with nominal point forecasts by finding a trade-off between conservative and risk-seeking policies. The case study uses the photovoltaic generation monitored on-site at the University of Liège (ULiège), Belgium.

**Index Terms**—Capacity firming, electricity market, robust optimization, energy management, renewable generation uncertainty, deep learning, normalizing flows.

## I. NOTATION

### Sets and indices

Name	Description
$t$	Time period index.
$T$	Number of time periods per day.
$\mathcal{T}$	Set of time periods, $\mathcal{T} = \{1, 2, \dots, T\}$ .
$\mathcal{P}$	Renewable generation uncertainty set.

### Variables

Name	Range	Description
$x_t$	$[X_t^{min}, X_t^{max}]$	Engagement, kW.
$y_t$	$[Y_t^{min}, Y_t^{max}]$	Net power, kW.
$y_t^G$	$[0, P_c]$	Renewable generation, kW.
$y_t^{cha}$	$[0, S^c]$	Charging power, kW.
$y_t^{dis}$	$[0, S^d]$	Discharging power, kW.
$y_t^s$	$[S^{min}, S^{max}]$	BESS state of charge, kWh.
$\delta x_t^-, \delta x_t^+$	$\mathbb{R}_+$	Under/overproduction, kW.
$y_t^b$	$\{0, 1\}$	BESS binary variable.
$z_t$	$\{0, 1\}$	Uncertainty set binary variable.

$\alpha_t$   $[M_t^-, M_t^+]$  Variables to linearize  $z_t \phi_t^{y^G}$ .

### Dual variables, and corresponding constraints

Dual variables of constraints are indicated with brackets  $[\cdot]$ .

Name	Range	Description
$\phi_t^{cha}, \phi_t^{dis}$	$\mathbb{R}^-$	Maximum (dis)charging. storage
$\phi_t^{S^{min}}, \phi_t^{S^{max}}$	$\mathbb{R}^-$	Minimum/maximum storage capacity.
$\phi_t^y$	$\mathbb{R}$	Net power balance.
$\phi_t^{Y^{min}}, \phi_t^{Y^{max}}$	$\mathbb{R}^-$	Minimum/maximum net power.
$\phi_t^{S^i}, \phi_t^{S^f}$	$\mathbb{R}^-$	Initial/final state of charge.
$\phi_t^{y^s}$	$\mathbb{R}^-$	BESS dynamics.
$\phi_t^{\delta x^-}, \phi_t^{\delta x^+}$	$\mathbb{R}^-$	Under/overproduction.
$\phi_t^{y^G}$	$\mathbb{R}^-$	Renewable generation.

### Parameters

Name	Description
$X_t^{min}, X_t^{max}$	Minimum/maximum engagement, kW.
$\Delta X_t$	Ramping-up and down limits for the engagement, kW.
$pP_c$	Engagement tolerance, $0 \leq p \leq 1$ , kW.
$y_t^m$	Net measured power, kW.
$Y_t^{min}, Y_t^{max}$	Minimum/maximum net power, kW.
$P_c$	Total installed capacity, kWp.
$\hat{p}_t, \hat{p}_t^{(q)}$	Point/quantile $q$ forecast, kW.
$p_t^{min}, p_t^{max}$	Uncertainty set lower/upper bounds, kW.
$S^d, S^c$	BESS maximum (dis)charging power, kW.
$\eta^d, \eta^c$	BESS (dis)charging efficiency.
$S^{min}, S^{max}$	BESS minimum/maximum capacity, kWh.
$S^i, S^f$	BESS initial/final state of charge, kWh.
$\pi_t$	Contracted selling price, €/kWh.
$\Delta t$	Duration of a time period, minutes.
$\Gamma$	Uncertainty budget.
$\beta$	Penalty factor.
$d_q, d_\Gamma$	Uncertainty and budget depths.
$M_t^-, M_t^+$	Big-M's values.

The authors are with the Departments of Computer Science and Electrical Engineering and Geography, University of Liège, 4000 Liège, Belgium, (e-mail: {jdumas, antoine.wehenkel, a.sutera, xavier.fettweis, bertrand.cornelusse}@uliege.be, colin.cointe@mines-paristech.fr).

## II. INTRODUCTION

THE capacity firming framework is mainly designed for isolated markets, such as the Overseas France islands. For instance, the French Energy Regulatory Commission (CRE) publishes capacity firming tenders and specifications. The system considered is a grid-connected renewable energy power plant, *e.g.*, photovoltaic or wind-based, with a battery energy storage system (BESS) for firming the renewable generation. At the tendering stage, offers are selected on the electricity selling price. Then, the successful tenderer builds its plant and sells the electricity exported to the grid at the contracted selling price, but according to a well-defined daily engagement and penalization scheme, specified in the tender specifications. The electricity to be injected in or withdrawn from the grid must be nominated the day-ahead, and engagements must satisfy ramping power constraints. The remuneration is calculated a posteriori by multiplying the realized exports by the contracted selling price minus a penalty. The deviations of the realized exports from the engagements are penalized through a function specified in the tender. A peak option can be activated in the contract for a significant selling price increase during a short period defined a priori. Therefore, the BESS is required to shift the renewable generation during peak hours to maximize revenue and to manage renewable energy uncertainty.

The problem of modeling a two-phase engagement/control with an approach dealing with uncertainty in the context of the CRE capacity framework is still an open issue. This framework has received less attention in the literature than more traditional energy markets such as day-ahead and intraday markets of European countries. There are several approaches to deal with renewable energy uncertainty. One way is to consider a two-stage stochastic programming approach [1]. It has already been applied to the capacity firming framework [2]–[5]. The generation uncertainty is captured by a set of scenarios modeling possible realizations of the power output. However, there are several difficulties to this approach: (1) the problem size and computational requirement increase with the number of scenarios, and a large number of scenarios are often required to ensure the good quality of the solution; (2) the accuracy of the algorithm is sensitive to the scenario generation technique. Another option is to consider robust optimization (RO) [6], [7]. RO has been applied to the unit commitment problem [8], [9] and once in the capacity firming context [3]. RO accounts for the worst scenario of generation to hedge the power output uncertainty, where the uncertainty model is deterministic and set-based. Indeed, the RO approach puts the random problem parameters in a predetermined uncertainty set containing the worst-case scenario. However, the RO version of a tractable optimization problem may not itself be tractable, and some care must be taken in the choice of the uncertainty set to ensure that tractability is preserved.

This paper proposes a reliable and computationally tractable probabilistic forecast-driven robust optimization strategy in the capacity firming framework, depicted in Figure 1. Our work goes several steps further than [3]. First, a recent deep learning technique, the *normalizing flows*, that defines a new class of probabilistic generative models that has gained increasing interest from the deep learning community in recent years is implemented. NFs are used to compute

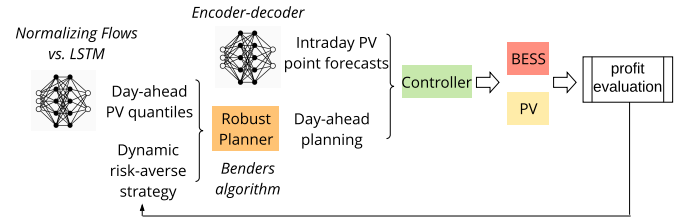


Fig. 1: Forecast-driven robust optimization strategy.

day-ahead quantiles of renewable generation for the robust planner. Then, an encoder-decoder architecture forecasting model [10] is used to compute intraday point forecasts for the controller. Second, the two-phase engagement/control problem is modeled with a RO planner using the quantile forecasts, and a controller using the day-ahead engagements and the intraday point forecasts. The non-linear robust optimization problem is solved using a Benders-dual cutting plane algorithm. The convergence is improved by building an initial set of cuts based on renewable generation trajectories assumed to be close to the worst trajectory. Third, the results of the RO planner are compared to the deterministic planner using perfect knowledge of the future, the nominal point forecasts, *i.e.*, the baseline to outperform, and the quantiles (a conservative approach). The case study is the photovoltaic (PV) generation monitored on-site at the University of Liège (ULiège), Belgium. Finally, a dynamic risk-averse parameters selection taking advantage of the quantile forecast distribution is investigated and compared to a strategy with fixed risk-averse parameters.

The main contributions of this paper are two-fold:

- 1) The core contribution is the application of the robust optimization framework to the capacity firming market in a tractable manner thanks to a Benders decomposition of the optimization problem and a warm start of the algorithm. In addition, a dynamic risk-averse parameters selection taking advantage of the quantile forecast distribution is proposed.
- 2) The secondary contribution is the use of the Normalizing Flows, which is a new advanced forecasting technique, to provide the uncertainty estimation in the form of PV quantiles for the robust planner. To the best of our knowledge, it is the first study to use NFs in a power system application.

The rest of the paper is organized as follows. Section III describes the capacity firming framework. Section IV provides the mathematical formulations of the robust and deterministic planners. Section V develops the Benders decomposition algorithm used to solve the robust formulation. The case study and computational results are shown in Section VI. Section VII concludes our research and draws some perspectives of future works. Finally, Appendix VIII introduces the forecasting techniques and proposes a quality evaluation.

### III. THE CAPACITY FIRING FRAMEWORK

The capacity firing framework can be decomposed into a day-ahead engagement process, Section III-A, and a real-time control process, Section III-B. Each day is discretized in  $T$  periods of duration  $\Delta t$ . In the sequel the time period duration is the same for day-ahead engagement and the real-time control,  $t$  is used as a time period index, and  $\mathcal{T}$  is the set of time periods in a day.

#### A. Day-ahead engagement

Each day, the operator of the renewable generation plant is asked to provide the generation profile to be followed the next day to the grid operator, based on renewable generation forecasts. More formally, a planner computes on a day-ahead basis, before a deadline, a vector of engagements composed of  $T$  values  $\{x_1, \dots, x_T\}$ . The engagements are accepted by the grid operator if they satisfy the constraints

$$|x_t - x_{t-1}| \leq \Delta X_t, \forall t \in \mathcal{T} \setminus \{1\} \quad (1a)$$

$$-x_t \leq -X_t^{\min}, \forall t \in \mathcal{T} \quad (1b)$$

$$x_t \leq X_t^{\max}, \forall t \in \mathcal{T}, \quad (1c)$$

where  $\forall t \in \mathcal{T} \setminus \{1\}$  is  $\mathcal{T}$  without the first time period,  $\Delta X_t$  a power ramping constraint, that is a fraction of the total installed capacity  $P_c$  determined at the tendering stage and imposed by the grid operator.

#### B. Real-time control

Then, in real-time, a receding-horizon controller computes at each period the generation level and the charge or discharge set-points from  $t$  to  $T$ , based on forecasts of renewable generation and the engagements. Only the set-points of the first period are applied to the system. The remuneration is calculated ex-post based on the realized power  $y_t^m$  at the grid coupling point. For a given control period, the net remuneration  $r_t$  of the plant is the gross revenue  $\Delta t \pi_t y_t^m$  minus a penalty  $c(x_t, y_t^m)$ , with  $\pi_t$  the contracted selling price set at the tendering stage

$$r_t = \Delta t \pi_t y_t^m - c(x_t, y_t^m), \forall t \in \mathcal{T}. \quad (2)$$

The penalty function  $c$  depends on the specifications of the tender. For the sake of simplicity in the rest of the paper,  $c$  is assumed to be symmetric, convex, and piecewise-linear.

### IV. OPTIMIZATION PROBLEMS FORMULATION

A two-stage robust optimization formulation is built to deal with the engagement for the uncertain renewable generation that is modeled with an uncertainty set. The deterministic and robust formulations of the planner are presented in Sections IV-A and IV-B. The robust optimization problem with recourse has the general form of a min-max-min optimization problem. The uncertainty set is defined by quantiles forecasts and a budget of uncertainty  $\Gamma$ . Section IV-C uses the dual of the inner problem to formulate a min-max optimization problem. Finally, Section IV-D presents the formulation of the controller.

#### A. Deterministic planner formulation

The objective function  $J$  to minimize is the opposite of the net revenue

$$J(x_t, y_t) = \sum_{t \in \mathcal{T}} \pi_t \Delta t [-y_t + \beta(\delta x_t^- + \delta x_t^+)], \quad (3)$$

with  $\beta$  a penalty factor. The deterministic formulation is the following Mixed-Integer Linear Program (MILP)

$$\min_{x_t \in \mathcal{X}, y_t \in \Omega(x_t, \hat{p}_t)} J(x_t, y_t), \quad (4)$$

where

$$\mathcal{X} = \{x_t : (5)\}$$

and

$$\Omega(x_t, \hat{p}_t) = \{y_t : (6) - (10)\}$$

are the sets of feasible engagements  $x_t$  and dispatch solutions  $y_t$  for a fixed engagement  $x_t$  and renewable generation point forecast  $\hat{p}_t$ . The optimization variables of (4) are the engagement variables  $x_t$ , the dispatch variables  $y_t$  (the net power at the grid connection point),  $y_t^{dis}$  (discharging power),  $y_t^{cha}$  (charging power),  $y_t^s$  (BESS state of charge),  $y_t^b$  (BESS binary variables),  $y_t^G$  (renewable generation), and  $\delta x_t^-, \delta x_t^+$  (threshold-linear penalty variables) (cf. Section I). From (1), the engagement constraints are<sup>1</sup>

$$x_t - x_{t-1} \leq \Delta X_t, \forall t \in \mathcal{T} \setminus \{1\} \quad (5a)$$

$$x_{t-1} - x_t \leq \Delta X_t, \forall t \in \mathcal{T} \setminus \{1\} \quad (5b)$$

$$-x_t \leq -X_t^{\min}, \forall t \in \mathcal{T} \quad (5c)$$

$$x_t \leq X_t^{\max}, \forall t \in \mathcal{T}. \quad (5d)$$

The set of constraints that bound  $y_t^{cha}$ ,  $y_t^{dis}$ , and  $y_t^s$  variables are  $\forall t \in \mathcal{T}$

$$y_t^{cha} \leq y_t^b S^c \quad [\phi_t^{cha}] \quad (6a)$$

$$y_t^{dis} \leq (1 - y_t^b) S^d \quad [\phi_t^{dis}] \quad (6b)$$

$$-y_t^s \leq -S^{\min} \quad [\phi_t^{S^{\min}}] \quad (6c)$$

$$y_t^s \leq S^{\max}, \quad [\phi_t^{S^{\max}}] \quad (6d)$$

where  $y_t^b$  are binary variables that prevent the simultaneous charge and discharge of the BESS. The power balance equation and the constraints on the net power at the grid connection point are  $\forall t \in \mathcal{T}$

$$y_t - y_t^G - (y_t^{dis} - y_t^{cha}) = 0 \quad [\phi_t^y] \quad (7a)$$

$$-y_t \leq -Y_t^{\min} \quad [\phi_t^{Y^{\min}}] \quad (7b)$$

$$y_t \leq Y_t^{\max}. \quad [\phi_t^{Y^{\max}}] \quad (7c)$$

<sup>1</sup>The ramping constraint on  $x_1$  is deactivated to decouple consecutive days of simulation. In reality, the updated value of the last engagement of the previous day would be taken to satisfy the constraint.

The dynamics of the BESS state of charge are <sup>2</sup>

$$y_1^s - \Delta t(\eta^c y_1^{cha} - \frac{y_1^{dis}}{\eta^d}) = S^i \quad [\phi^{S^i}] \quad (8a)$$

$$y_t^s - y_{t-1}^s - \Delta t(\eta^c y_t^{cha} - \frac{y_t^{dis}}{\eta^d}) = 0, \quad [\phi_t^{y^s}] \quad (8b)$$

$$y_T^s = S^f = S^i. \quad [\phi^{S^f}] \quad (8c)$$

The variables  $\delta x_t^-, \delta x_t^+$  are defined  $\forall t \in \mathcal{T}$  to model the symmetric threshold-linear penalty

$$-\delta x_t^- \leq (y_t - (x_t - pP_c)) \quad [\phi_t^{\delta x^-}] \quad (9a)$$

$$-\delta x_t^+ \leq ((x_t + pP_c) - y_t), \quad [\phi_t^{\delta x^+}] \quad (9b)$$

with  $0 \leq p \leq 1$ . Finally, the renewable generation is bounded by the point forecast  $\hat{p}_t \forall t \in \mathcal{T}$

$$y_t^G \leq \hat{p}_t. \quad [\phi_t^{y^G}] \quad (10)$$

### B. Robust planner formulation

The uncertain renewable generation  $\hat{p}_t$  of (10) is assumed to be within an interval  $[p_t^{min}, p_t^{max}]$  that can be obtained based on the historical data or an interval forecast composed of quantiles. In the capacity firming framework, where curtailment is allowed, the uncertainty interval consists only in short deviation  $[p_t^{min}, \hat{p}_t^{(0.5)}]$ , with  $\hat{p}_t^{(0.5)}$  the 50 % quantile.

*Demonstration 1:* Let consider  $\mathcal{P}_1 = [p_t^{min}, \hat{p}_t^{(0.5)}]$ ,  $\mathcal{P}_2 = [\hat{p}_t^{(0.5)}, p_t^{max}]$ ,  $\hat{p}_t \in \mathcal{P}_1$ , and  $\hat{p}_t^2 \in \mathcal{P}_2$ . It is obvious  $\hat{p}_t^1 \leq \hat{p}_t^2 \forall t \in \mathcal{T}$ . Then, let consider  $y_t^1 \in \Omega_1 = \Omega(x_t, \hat{p}_t^1 \in \mathcal{P}_1)$  and  $y_t^2 \in \Omega_2 = \Omega(x_t, \hat{p}_t^2 \in \mathcal{P}_2)$ . The only difference between  $\Omega_1$  and  $\Omega_2$  is (10) where  $y_t^{G,1} \leq \hat{p}_t^1$  and  $y_t^{G,2} \leq \hat{p}_t^2$ . However, as  $\hat{p}_t^1 \leq \hat{p}_t^2$ , it is straightforward that  $y_t^{G,1} \leq \hat{p}_t^2$ . Therefore,  $y_t^1 \in \Omega_2 \forall t \in \mathcal{T}$ , and  $\Omega_1 \subseteq \Omega_2$ . Thus,  $\min_{y_t \in \Omega_2} J(x_t, y_t) = J_2^* \leq \min_{y_t \in \Omega_1} J(x_t, y_t) = J_1^*$ , and  $\max(J_2^*, J_1^*) = J_1^*$ . It means the worst case is in  $\Omega_1$  that corresponds to  $\mathcal{P}_1$ .

To adjust the degree of conservatism, a budget of uncertainty parameter  $\Gamma$  [11] taking integer values between 0 and 95 is employed to restrict the number of time periods that allow  $\hat{p}_t$  to be far away from its nominal value, *i.e.*, deviations are very large. Therefore, the uncertainty set of renewable generation  $\mathcal{P}$  is defined as follows

$$\mathcal{P} = \{p_t \in \mathbb{R}^T : \sum_{t \in \mathcal{T}} z_t \leq \Gamma, z_t \in \{0, 1\} \forall t \in \mathcal{T}, p_t = \hat{p}_t^{(0.5)} - z_t p_t^{min} \forall t \in \mathcal{T}\}, \quad (11)$$

where  $p_t^{min} = \hat{p}_t^{(0.5)} - \hat{p}_t^{(q)}$ , with  $0 \leq q \leq 0.5$ . When  $\Gamma = 0$ , the uncertainty set  $\mathcal{P} = \{\hat{p}_t^{(0.5)}\}$  is a singleton, corresponding to the nominal deterministic case. As  $\Gamma$  increases the size of  $\mathcal{P}$  enlarges. This means that a larger total deviation from the expected renewable generation is considered, so that the resulting robust solutions are more conservative and the system is protected against a higher degree of uncertainty. When  $\Gamma = T$ ,  $\mathcal{P}$  spans the entire hypercube defined by the intervals

<sup>2</sup>The parameters  $S^f$  and  $S^i$  are introduced to decouple consecutive days of simulation. In reality,  $S^i$  would be the updated value of the last measured state of charge of the previous day.

for each  $p_t$ . With this uncertainty set description, the proposed two-stage robust formulation of the capacity firming problem consists of minimizing the objective function over the worst renewable generation trajectory

$$\max_{\hat{p}_t \in \mathcal{P}} \left[ \min_{x_t \in \mathcal{X}, y_t \in \Omega(x_t, \hat{p}_t)} J(x_t, y_t) \right], \quad (12)$$

that is equivalent to

$$\min_{x_t \in \mathcal{X}} \left[ \max_{\hat{p}_t \in \mathcal{P}} \min_{y_t \in \Omega(x_t, \hat{p}_t)} J(x_t, y_t) \right]. \quad (13)$$

The worst-case dispatch cost has a max-min form, where

$$\min_{y_t \in \Omega(x_t, \hat{p}_t)} J(x_t, y_t)$$

determines the economic dispatch cost for a fixed engagement and a renewable generation trajectory, which is then maximized over the uncertainty set  $\mathcal{P}$ .

### C. Second-stage planner transformation

The proposed formulation (13) consists of solving a min-max-min problem, which cannot be solved directly by a commercial software such as CPLEX or GUROBI. A scenario-based approach, *e.g.*, enumerating all possible outcomes of  $\hat{p}_t$  that could lead to the worst-case scenario for the problem, results in at least  $2^\Gamma$  possible trajectories<sup>3</sup>. Thus, to deal with the huge size of the problem a decomposition algorithm is used to solve the problem [8], [9], [12].

Constraints (6a)-(6b) make the dispatch problem a MILP, for which a dual formulation cannot be derived. In view of this, following [9], the constraints (6a)-(6b) are relaxed. However, at the end of the optimization process the solution is checked to ensure there is no simultaneous charge and discharge, that never happens when the (dis)charge efficiencies are smaller than 1. By applying standard tools of duality theory in linear programming, the constraints and the objective function of the dual of the dispatch problem are derived. The dual of the feasible set  $\Omega(x_t, \hat{p}_t)$ , with (6a)-(6b) relaxed, provides the dual variables  $\phi_t$  and the following objective

$$G(x_t, \hat{p}_t, \phi_t) = \sum_{t \in \mathcal{T}} \left[ \phi_t^{cha} S^c + \phi_t^{dis} S^d - \phi_t^{S^{min}} S^{min} + \phi_t^{S^{max}} S^{max} - \phi_t^{Y^{min}} Y^{min} + \phi_t^{Y^{max}} Y^{max} + \phi^{S^i} S^i + \phi^{S^f} S^f - \phi_t^{\delta x^-} (x_t - pP_c) + \phi_t^{\delta x^+} (x_t + pP_c) + \phi_t^{y^G} \hat{p}_t \right]. \quad (14)$$

Then, the dual of the dispatch problem  $\min_{y_t \in \Omega(x_t, \hat{p}_t)} J(x_t, y_t)$  is

$$\max_{\phi_t \in \Phi} G(x_t, \hat{p}_t, \phi_t), \quad (15)$$

<sup>3</sup>There are  $n = \sum_{k=0}^{\Gamma} \binom{96}{k}$  possible trajectories where  $n$  is within the interval  $[2^\Gamma, 2^{96}]$  as  $(1+1)^\Gamma = \sum_{k=0}^{\Gamma} \binom{\Gamma}{k}$  and  $(1+1)^{96} = \sum_{k=0}^{96} \binom{96}{k}$  by using the binomial formula.

with the set of constraints  $\Phi$  defined by

$$\phi_t^y - \phi_t^{Y^{min}} + \phi_t^{Y^{max}} - \phi_t^{\delta x^-} + \phi_t^{\delta x^+} = -\pi_t \Delta t, \quad \forall t \in \mathcal{T} \quad [y_t] \quad (16a)$$

$$-\phi_t^{\delta x^-} \leq \beta \pi_t \Delta t, \quad \forall t \in \mathcal{T} \quad [\delta x_t^-] \quad (16b)$$

$$-\phi_t^{\delta x^+} \leq \beta \pi_t \Delta t, \quad \forall t \in \mathcal{T} \quad [\delta x_t^+] \quad (16c)$$

$$\phi_1^{dis} - \phi_1^y + \phi_1^{S^i} \frac{\Delta t}{\eta^d} \leq 0 \quad [y_1^{dis}] \quad (16d)$$

$$\phi_t^{dis} - \phi_t^y + \phi_t^{y^s} \frac{\Delta t}{\eta^d} \leq 0, \quad \forall t \in \mathcal{T} \setminus \{1\} \quad [y_t^{dis}] \quad (16e)$$

$$\phi_1^{cha} + \phi_1^y - \phi_1^{S^i} \eta^c \Delta t \leq 0 \quad [y_1^{cha}] \quad (16f)$$

$$\phi_t^{cha} + \phi_t^y - \phi_t^{y^s} \eta^c \Delta t \leq 0, \quad \forall t \in \mathcal{T} \setminus \{1\} \quad [y_t^{cha}] \quad (16g)$$

$$-\phi_1^{S^{min}} + \phi_1^{S^{max}} + \phi_1^{S^i} - \phi_2^{y^s} \leq 0 \quad [y_1^s] \quad (16h)$$

$$-\phi_t^{S^{min}} + \phi_t^{S^{max}} + \phi_{t-1}^{y^s} - \phi_t^{y^s} \leq 0, \quad \forall t \in \mathcal{T} \setminus \{1, 2, T\} \quad [y_t^s] \quad (16i)$$

$$-\phi_T^{S^{min}} + \phi_T^{S^{max}} + \phi_T^{S^f} + \phi_T^{y^s} \leq 0 \quad [y_T^s] \quad (16j)$$

$$-\phi_t^y + \phi_t^{y^G} \leq 0, \quad \forall t \in \mathcal{T}, \quad [y_t^G]. \quad (16k)$$

The worst-case dispatch problem  $\max_{\hat{p}_t \in \mathcal{P}} [\min_{y_t \in \Omega(x_t, \hat{p}_t)} J(x_t, y_t)]$  is equivalent to

$$R(x_t) = \max_{\hat{p}_t \in \mathcal{P}, \phi_t \in \Phi} G(x_t, \hat{p}_t, \phi_t). \quad (17)$$

Overall, (13) becomes a min-max problem

$$\min_{x_t \in \mathcal{X}} \left[ \max_{\hat{p}_t \in \mathcal{P}, \phi_t \in \Phi} G(x_t, \hat{p}_t, \phi_t) \right], \quad (18)$$

that can be solved using a Benders decomposition [8], [9], between a master problem, that is linear, and a sub-problem, that is bilinear. Indeed,  $G$  has the following bilinear terms  $\phi_t^{y^G} \hat{p}_t = \phi_t^{y^G} \hat{p}_t^{(0.5)} - \phi_t^{y^G} z_t p_t^{min}$ . It is possible to linearize the products of the binary and continuous variables  $z_t \phi_t^{y^G}$  of  $G$  by using a standard integer algebra trick [13] with the following constraints  $\forall t \in \mathcal{T}$

$$-M_t^- z_t \leq \alpha_t \leq M_t^+ z_t \quad (19a)$$

$$-M_t^-(1 - z_t) \leq \phi_t^{y^G} - \alpha_t \leq M_t^+(1 - z_t), \quad (19b)$$

where  $M_t^\pm$  are the big-M's values of  $\phi_t^{y^G}$  and  $\alpha_t$  is an auxiliary continuous variable.

#### D. Controller formulation

The controller uses as parameters the engagements  $x_t$ , the system last measured values, and renewable generation intraday point forecasts. It computes at each time period  $t$  the setpoints from  $t$  to the last period  $T$  of the day. The formulation is the following MILP

$$\min_{y_t \in \Omega(x_t, \hat{p}_t)} J(x_t, y_t). \quad (20)$$

### V. SOLUTION METHODOLOGY

Following the methodology described by [8], [9], a two-level algorithm can be used to solve the RO problem with a Benders-dual cutting plane algorithm. The following master

problem (MP) is solved iteratively by adding new constraints to cut off the infeasible or non-optimal solutions

$$\min_{x_t \in \mathcal{X}, \theta} \theta \quad (21a)$$

$$\theta \geq G(x_t, \alpha_{t,l}, \phi_{t,l}), \quad l = 1 \dots L \quad (21b)$$

$$G(x_t, \tilde{\alpha}_{t,k}, \tilde{\phi}_{t,k}) \leq 0, \quad k = 1 \dots K, \quad (21c)$$

where constraints (21b) represent the optimality cuts, generated by retrieving the optimal values  $\alpha_{t,l}, \phi_{t,l}$  of (17), while constraints (21c) represent the feasibility cuts, generated by retrieving the extreme rays  $\tilde{\alpha}_{t,k}, \tilde{\phi}_{t,k}$  of (17), and  $\theta$  is the optimal value of the second-stage problem.

#### A. Convergence warm start

A warm start algorithm is used to improve the Benders convergence by building an initial set of cuts  $\{\theta_i\}_{1 \leq i \leq I}$  for the master problem (21). It consists of sampling renewable generation trajectories that are assumed to be close to the worst trajectory of  $\mathcal{P}$ . Let  $t_1$  and  $t_f$  be the time periods corresponding to the first and last non null 50 % quantile values. If  $m = t_f - (t_1 + \Gamma - 1) > 0$ ,  $m$  trajectories are sampled. The  $m^{\text{th}}$  sampled trajectory is built by setting the  $\Gamma$  values of the 50 % quantile to the  $p_t^{min}$  lower bound for time periods  $t_1 + (m - 1) \leq t \leq t_1 + \Gamma - 1 + (m - 1)$ . An additional trajectory is built by setting the  $\Gamma$  maximum values of the 50 % quantile to  $p_t^{min}$  lower bound. Then, for each sampled trajectory  $p_{t,i}$ , the MILP formulation (4) is used to compute the related engagement plan  $x_{t,i}$ . Finally, the cut  $\theta_i$  is built by solving (17) where the uncertainty set is a singleton  $\mathcal{P} = \{p_{t,i}\}$ , and the engagement plan is  $x_{t,i}$  to retrieve the optimal values with (21b):  $\theta_i = G(x_{t,i}, \alpha_{t,i}, \phi_{t,i})$ ,  $i = 1 \dots I$ .

#### B. Convergence check

The objective of the master problem at the last Benders iteration  $J$  is compared to the objective of the MILP formulation (4), using the generation worst-case trajectory of the last Benders iteration as parameters. If the absolute gap is higher than a convergence threshold then larger big-M's values are set, and the Benders algorithm is executed until convergence. Therefore, this process guarantees to achieve the Benders algorithm convergence towards the optimal solution, given the threshold.

#### C. Algorithm framework

The Benders-dual cutting plane algorithm, depicted in Figure 2, consists of solving (18) without constraints [(6a)-(6b)] following the procedure previously described, and to obtain a day-ahead robust schedule  $x_{t,J}$ . The initialization step consists of setting the initial big-M's values  $M_t^- = 1$  and  $M_t^+ = 0 \quad \forall t \in \mathcal{T}$ , the time limit resolution of the subproblem (17) to 10 s, and the threshold convergence  $\epsilon$  to 0.5 €. Let  $MP^j, SP^j$ , be the MP and SP objective values at iteration  $j$ , and  $MILP^j$  the MILP objective value using the worst renewable generation trajectory  $p_{t,J}$  at the last Benders algorithm iteration  $J$ .



Initialization.

Build the initial set of cuts  $\{\theta_i\}_{1 \leq i \leq I}$ .

**while**  $|MILP^J - MP^J| > \epsilon$  **do**

Initialize  $j = 0$ .

Solve the MP (21) and retrieve  $x_{t,0}$ .

**while** the 10 last  $|MP^j - SP^j|$  are not  $< \epsilon$  **do**

Solve the SP (17):

**if** the SP is unbounded **then**

Retrieve the extreme rays  $\tilde{\alpha}_{t,k}, \tilde{\phi}_{t,k}, 0 \leq k \leq j$ .

Add the  $k^{th}$  feasibility cut:

$$G(x_{t,j}, \tilde{\alpha}_{t,k}, \tilde{\phi}_{t,k}) \leq 0.$$

**else**

Retrieve the optimal values  $\alpha_{t,l}, \phi_{t,l}, 0 \leq l \leq j$ .

Add the  $l^{th}$  optimality cut:

$$\theta \geq G(x_{t,j}, \alpha_{t,l}, \phi_{t,l}).$$

Update  $SP^j = R(x_{t,j})$ .

**end if**

Solve the MP (21).

Retrieve the optimal values  $\theta_j, x_{t,j}$ .

Update  $MP^j = \theta_j$ .

Update the engagement  $x_{t,j+1} = x_{t,j}$ .

**end while**

Convergence checking at the last Benders iteration  $J$ :

**if**  $|MILP^J - MP^J| > \epsilon$  **then**

Update big-M's values  $M_t^- = 10 + M_t^- \forall t \in \mathcal{T}$ .

**end if**

**end while**

Fig. 2: Benders-style cutting plane algorithm.

## VI. CASE STUDY

The ULiège case study is composed of a PV generation plant with an installed capacity  $P_c = 466.4$  kWp. The PV generation is monitored on a minute basis and the data are resampled to 15 minutes. The dataset is composed of 350 days from August 2019 to November 2020, missing data during March 2020. The NFs approach is compared to a widely used neural architecture, referred to as Long Short-Term Memory (LSTM). In total six versions of the planner are considered. Two versions of the robust optimization planner, using the Benders decomposition algorithm, with the NFs and the LSTM PV quantiles. Four deterministic versions of the deterministic optimization planner: the oracle that uses perfect knowledge of the future, a benchmark that uses PV nominal point forecasts, and two versions using NFs and LSTM PV quantiles. Note, the profits are normalized by the profit of the oracle and expressed in %. The set of PV quantiles considered is  $\mathcal{Q} = \{q = 10\%, \dots, 50\%\}$ .

Section VI-A presents the numerical settings. Section VI-B provides the results of the sensitivity analysis for several risk-averse pairs  $[p_t^{min} = \hat{p}^{(q)}, \Gamma]$ , with  $q = 10, \dots, 40\%$ , and  $\Gamma = 12, 24, 36, 48$ . Section VI-C investigates a dynamic risk-averse parameter selection. Finally, Section VI-D presents the improvement in terms of computation time provided by the initial set of cuts.

### A. Numerical settings

30 random days are randomly selected from the dataset to compose the testing set. The simulation parameters of the planners and the controller are identical. The planning and controlling time periods duration are  $\Delta t = 15$  minutes. The peak hours are set between 7 pm and 9 pm (UTC+0). The ramping power constraint on the engagements are  $\Delta X_t = 7.5\%P_c$  ( $15\%P_c$ ) during off-peak (peak) hours. The lower bounds on the engagement  $X_t^{min}$  and the net power  $Y_t^{min}$  are set to 0 kW. The upper bound on the engagement  $X_t^{max}$  and the net power  $Y_t^{max}$  are set to  $P_c$ . Finally, the engagement tolerance is  $pP_c = 1\%P_c$ , and the penalty factor  $\beta = 5$ . The BESS minimum  $S^{min}$  and maximum capacity are 0 kWh and 466.4 kWh, respectively. It is assumed to be capable of fully charging or discharging in one hour  $S^d = S^c = S^{max}/1$  with charging and discharging efficiencies  $\eta^d = \eta^c = 95\%$ . Each simulation day is independent with a fully discharged battery at the first and last period  $S^i = S^f = 0$  kWh. The Python Gurobi library is used to implement the algorithms in Python 3.7, and Gurobi<sup>4</sup> 9.0.2 to solve all the optimization problems. Numerical experiments are performed on an Intel Core i7-8700 3.20 GHz based computer with 12 threads and 32 GB of RAM running on Ubuntu 18.04 LTS.

Figures 3a and 3b illustrate the LSTM and NFs PV quantile forecasts, observation, and nominal point forecasts on September 14, 2019. Figures 3c and 3d provide the engagement plan (x) and the BESS state of charge (s) computed with the RO planner, the deterministic planner with the nominal point forecasts, and the perfect knowledge of the future.

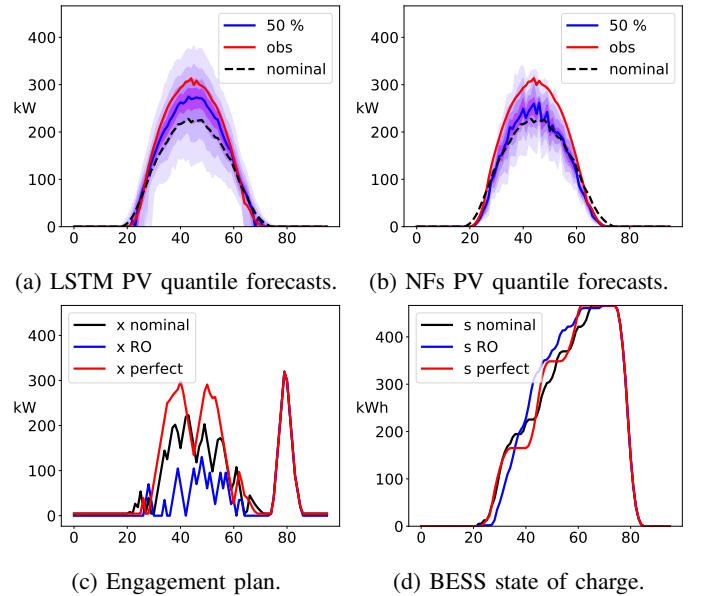


Fig. 3: Results illustration on September 14, 2019.

### B. Constant risk-averse parameters strategy

The risk-averse parameters of the RO approach  $[\hat{p}^{(q)}, \Gamma]$  are constant over the dataset. One way to identify the optimal pair

<sup>4</sup><https://www.gurobi.com/>

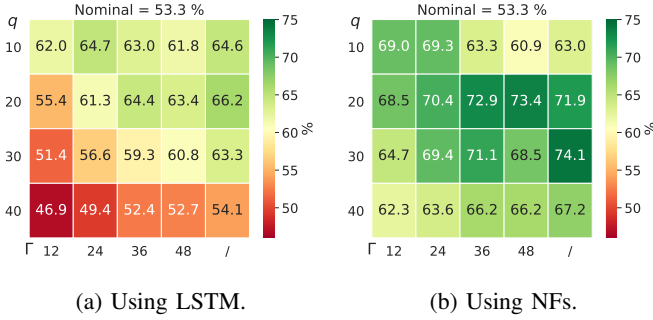


Fig. 4: Normalized profit (%) of RO ( $[\Gamma, q]$ ) and deterministic ( $[\cdot, q]$ ) planners with constant risk-averse parameters.

is to perform a sensitivity analysis [14]. Figure 4 provides the normalized profits of the RO and deterministic planners using PV quantiles, left with LSTM and right with NFs, and nominal point forecasts. Both using the LSTM and NFs quantiles, the RO and deterministic planners outperform by a large margin the deterministic planner with nominal point forecasts that cannot deal with PV uncertainty and achieved only 53.3 %. Then, the planners using NFs quantiles significantly outperform the planners with LSTM quantiles. The highest profits achieved by the RO and deterministic planners using NFs quantiles are 73.4 % and 74.1 %, respectively, with the pair  $[q = 20\%, \Gamma = 48]$  and the quantile 30 %. It should be possible to improve the RO results by tuning the risk-averse parameters  $[\hat{p}_t^{(q)}, \Gamma]$ . However, these results emphasize the interest to consider a deterministic planner with the relevant PV quantile as point forecasts, that is easy to implement, fast to compute (a few seconds), and less prone to convergence issues than the RO approach.

### C. Dynamic risk-averse parameters strategy

In this section, the risk-averse parameters  $[p_t^{min}, \Gamma]$  of the RO approach are dynamically set based on the day-ahead quantile forecasts distribution, and  $p_t^{min}$  is not necessarily equal to the same quantile  $\hat{p}_t^{(q)} \forall t \in \mathcal{T}$ . The motivation of this strategy is to assume that the sharper the quantile forecast distribution around the median is, the more risk-averse the RO approach should be.

Two parameters are designed to this end: (1) the PV uncertainty set max depth  $d_q$  to control  $p_t^{min}$ ; (2) the budget depth  $d_\Gamma$  to control  $\Gamma$ .  $d_q$  is a percentage of the distance between the median and the 10 % quantile  $d_{50-10}$ , and  $d_\Gamma$  is a percentage of the total installed capacity  $P_c$ . Then, two rules are designed to dynamically set the risk-averse parameters  $[p_t^{min}, \Gamma]$  for each day of the dataset. For a given day, and the set of time periods where the PV median is non null, the distances between the PV median and the PV quantiles 20, 30, and 40 % are computed:  $d_{50-20}$ ,  $d_{50-30}$ ,  $d_{50-40}$ .  $p_t^{min}$  is dynamically set at each time period  $t$  as follows

$$p_t^{min} = \begin{cases} \hat{p}_t^{(0.1)} & \text{if } d_t^{50-20/30/40} > d_q d_t^{50-10} \\ \hat{p}_t^{(0.2)} & \text{if } d_t^{50-20/30} > d_q d_t^{50-10} \\ \hat{p}_t^{(0.3)} & \text{if } d_t^{50-20} > d_q d_t^{50-10} \\ \hat{p}_t^{(0.4)} & \text{otherwise} \end{cases} \quad (22)$$

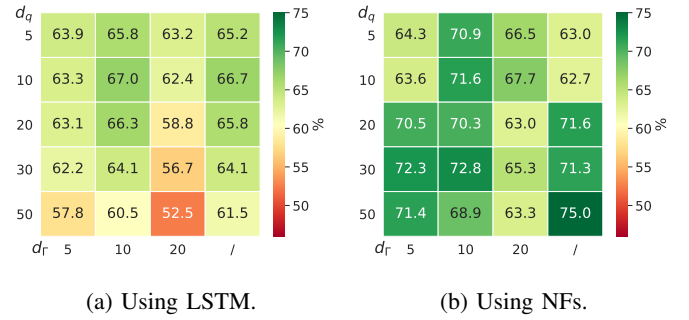


Fig. 5: Normalized profit (%) of RO ( $[d_\Gamma, d_q]$ ) and deterministic ( $[\cdot, d_q]$ ) planners with dynamic risk-averse parameters.

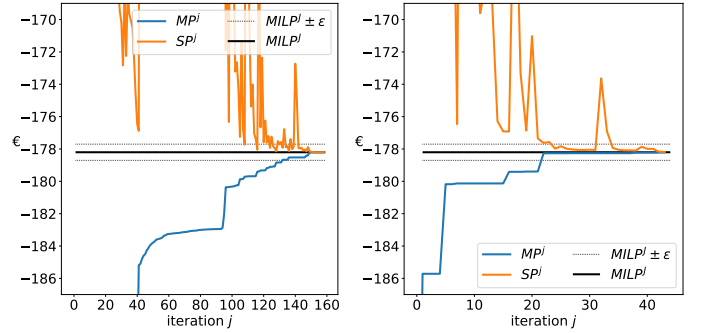


Fig. 6: Benders convergence without (left) and with (right) an initial set of cuts on September 14, 2019.

For a given day, the budget of uncertainty  $\Gamma$  is dynamically set based on the following rule

$$\Gamma = \#\{t : d_t^{50-10} > d_\Gamma P_c\}. \quad (23)$$

Figure 5 provides the normalized profits of the RO and deterministic planners for several pairs  $[d_\Gamma, d_q]$  using both the LSTM and NFs quantiles. When considering the LSTM quantiles, the results are improved in comparison with fixed risk-averse parameters. The RO approach achieved the highest profit of 67.0 % and the deterministic planner of 66.7 %, with  $[d_\Gamma, d_q] = [10, 10]$  and  $d_q = 10\%$ , respectively. When considering the NFs quantiles, only the deterministic planner achieved a higher profit of 75.0 % than with fixed risk-averse parameters.

### D. Convergence warm start improvement

The initial set of cuts impact on the convergence is assessed by considering the dynamic risk-averse parameters strategy with  $[d_\Gamma, d_q] = [10, 10]$ . Figure 6 illustrates the reduction of the total number of iteration  $J$  required to converge below the threshold  $\epsilon$ , on a specific day of the dataset, that is divided by 3.6 from 159 to 44. The computation time is divided by 4.1 from 7.4 min to 1.8 min. Table I provides the computation times (min) statistics over the entire dataset with and without warm start. The averaged  $t^{av}$  and total  $t^{tot}$  computation times are reduced significantly when using the initial set of cuts.

$\{\theta_i\}_{1 \leq i \leq I}$	$t^{av}$	$t^{50\%}$	$t^{min}$	$t^{max}$	$t^{tot}$
False	3.5	2.0	< 0.1	34.1	105.4
True	2.0	0.7	< 0.1	30.4	61.3

TABLE I: Computation times (min) statistics.

## VII. CONCLUSION

The core contribution of this study is to address the two-phase engagement/control problem in the context of capacity firming. We developed an integrated forecast-driven strategy modeled as a min-max-min robust optimization problem with recourse and solved the resulting optimization problem using a Benders-dual cutting plane algorithm. The convergence is improved by warm starting the algorithm with an initial set of cuts, and the convergence is checked by ensuring a gap below a threshold between the final objective and the corresponding deterministic objective value. A risk-averse parameter assessment is conducted to select the optimal robust parameters and the optimal conservative quantile for the deterministic planner. Both the NFs-based and LSTM-based planners outperformed the deterministic planner with nominal point PV forecasts. The NFs model outperforms the LSTM in terms of forecast value as the planner using the NFs quantiles achieved higher profit than the planner with LSTM quantiles. Finally, a dynamic risk-averse parameter selection strategy is built by taking advantage of the PV quantile forecast distribution. Overall, the RO approach allows finding a trade-off between conservative and risk-seeking policies by selecting the optimal robust optimization parameters, leading to improved economic benefits in comparison with the baseline. Therefore, offering a probabilistic guarantee for the robust solution. However, the deterministic planner with the relevant PV quantile achieved interesting results. It emphasizes the interest to consider a well-calibrated deterministic approach, easy to implement, computationally tractable for large scale problem, and less prone to convergence issues, that is not considered in [3]. Note, this approach can be used in any other case study. It only requires a few months of data, renewable generation and weather forecasts, to train the forecasting models to compute reliable forecasts for the planner.

A secondary contribution is to use a recent deep learning technique, Normalizing Flows, to compute PV quantiles. It is compared to a common neural architecture, referred to as Long Short-Term Memory. The NFs model outperforms the LSTM in terms of forecast quality by using the quantile score, reliability diagram, and continuous rank probability score.

Several extensions are under investigation: (1) a stochastic formulation of the planner with improved PV scenarios based on Gaussian copula methodology or generated by a state-of-the-art deep learning technique such as Normalizing Flows, Generative Adversarial Networks or Variational AutoEncoders; (2) an improved dynamic risk-averse parameter selection strategy based on a machine learning tool capable of better-taking advantage of the PV quantiles distribution; (3) the comparison of the proposed approach with a column and constraints generation algorithm that is said to be more

effective in terms of iterations to converge [15].

## ACKNOWLEDGMENT

The authors thank Quentin Louveaux, associate professor at Liège University, to help to propose demonstration 1. In addition, the authors would like to thank the editor and the reviewers for the comments that help to improve the paper. Antoine Wehenkel, recipient of a F.R.S.- FNRS fellowship, and Xavier Fettweis, FNRS research associate, acknowledge the financial support of the FNRS (Belgium). Antonio Sutera is supported via the Energy Transition Funds project EPOC 2030-2050 organized by the FPS economy, S.M.E.s, Self-employed and Energy.

## REFERENCES

- [1] J. R. Birge and F. Louveaux, *Introduction to stochastic programming*. Springer Science & Business Media, 2011.
- [2] J. Dumas, B. Cornélusse, X. Fettweis, A. Giannitrapani, S. Paoletti, and A. Vicino, "Probabilistic forecasting for sizing in the capacity firming framework," 2021, (in press in proceedings of 2021 IEEE Madrid PowerTech).
- [3] A. N'Goran, "Contrôle optimal et gestion énergétique d'une station d'énergie autonome par optimisation robuste," Ph.D. dissertation, Université Paris sciences et lettres, 2020.
- [4] P. Haessig, "Dimensionnement et gestion d'un stockage d'énergie pour l'atténuation des incertitudes de production éolienne," Ph.D. dissertation, Cachan, Ecole normale supérieure, 2014.
- [5] A. Parisio, E. Rikos, and L. Glielmo, "Stochastic model predictive control for economic/environmental operation management of microgrids: An experimental case study," *Journal of Process Control*, vol. 43, pp. 24–37, 2016.
- [6] A. Ben-Tal, L. El Ghaoui, and A. Nemirovski, *Robust optimization*. Princeton University Press, 2009, vol. 28.
- [7] D. Bertsimas, D. B. Brown, and C. Caramanis, "Theory and applications of robust optimization," *SIAM review*, vol. 53, no. 3, pp. 464–501, 2011.
- [8] D. Bertsimas, E. Litvinov, X. A. Sun, J. Zhao, and T. Zheng, "Adaptive robust optimization for the security constrained unit commitment problem," *IEEE transactions on power systems*, vol. 28, no. 1, pp. 52–63, 2012.
- [9] R. Jiang, J. Wang, and Y. Guan, "Robust unit commitment with wind power and pumped storage hydro," *IEEE Transactions on Power Systems*, vol. 27, no. 2, pp. 800–810, 2011.
- [10] J. Bottieau, L. Hubert, Z. De Grève, F. Vallée, and J.-F. Toubeau, "Very-short-term probabilistic forecasting for a risk-aware participation in the single price imbalance settlement," *IEEE Transactions on Power Systems*, vol. 35, no. 2, pp. 1218–1230, 2019.
- [11] D. Bertsimas and M. Sim, "The price of robustness," *Operations research*, vol. 52, no. 1, pp. 35–53, 2004.
- [12] J. M. Morales, A. J. Conejo, H. Madsen, P. Pinson, and M. Zugno, *Integrating renewables in electricity markets: operational problems*. Springer Science & Business Media, 2013, vol. 205.
- [13] I. Savelli, B. Cornélusse, A. Giannitrapani, S. Paoletti, and A. Vicino, "A new approach to electricity market clearing with uniform purchase price and curtailable block orders," *Applied energy*, vol. 226, pp. 618–630, 2018.
- [14] R. Wang, P. Wang, and G. Xiao, "A robust optimization approach for energy generation scheduling in microgrids," *Energy Conversion and Management*, vol. 106, pp. 597–607, 2015.
- [15] B. Zeng and L. Zhao, "Solving two-stage robust optimization problems using a column-and-constraint generation method," *Operations Research Letters*, vol. 41, no. 5, pp. 457–461, 2013.
- [16] D. Rezende and S. Mohamed, "Variational inference with normalizing flows," in *International Conference on Machine Learning*. PMLR, 2015, pp. 1530–1538.
- [17] G. Papamakarios, E. Nalisnick, D. J. Rezende, S. Mohamed, and B. Lakshminarayanan, "Normalizing flows for probabilistic modeling and inference," *arXiv preprint arXiv:1912.02762*, 2019.
- [18] A. Oord, Y. Li, I. Babuschkin, K. Simonyan, O. Vinyals, K. Kavukcuoglu, G. Driessche, E. Lockhart, L. Cobo, F. Stimberg et al., "Parallel wavenet: Fast high-fidelity speech synthesis," in *International conference on machine learning*. PMLR, 2018, pp. 3918–3926.



- [19] M. S. Albergo, D. Boyda, D. C. Hackett, G. Kanwar, K. Cranmer, S. Racanière, D. J. Rezende, and P. E. Shanahan, "Introduction to normalizing flows for lattice field theory," *arXiv preprint arXiv:2101.08176*, 2021.
- [20] L. Ge, W. Liao, S. Wang, B. Bak-Jensen, and J. R. Pillai, "Modeling daily load profiles of distribution network for scenario generation using flow-based generative network," *IEEE Access*, vol. 8, pp. 77 587–77 597, 2020.
- [21] A. Wehenkel and G. Louppe, "Unconstrained monotonic neural networks," in *Advances in Neural Information Processing Systems*, 2019, pp. 1545–1555.
- [22] X. Fettweis, J. Box, C. Agosta, C. Amory, C. Kittel, C. Lang, D. van As, H. Machguth, and H. Gallée, "Reconstructions of the 1900–2015 greenland ice sheet surface mass balance using the regional climate MAR model," *Cryosphere (The)*, vol. 11, pp. 1015–1033, 2017.
- [23] T. Gneiting and A. E. Raftery, "Strictly proper scoring rules, prediction, and estimation," *Journal of the American statistical Association*, vol. 102, no. 477, pp. 359–378, 2007.
- [24] M. Zamo and P. Naveau, "Estimation of the continuous ranked probability score with limited information and applications to ensemble weather forecasts," *Mathematical Geosciences*, vol. 50, no. 2, pp. 209–234, 2018.
- [25] P. Lauret, M. David, and P. Pinson, "Verification of solar irradiance probabilistic forecasts," *Solar Energy*, vol. 194, pp. 254–271, 2019.

### VIII. APPENDIX: FORECASTING TECHNIQUES

The processes described in Section III require day-ahead and intraday *top-quality* forecasts. The more accurate the forecasts, the better the planning and the control. The robust optimization-based approach needs quantile forecasts to define the uncertainty interval. To this end, the Normalizing Flows technique is used to compute quantile day-ahead forecasts that are compared to a common alternative technique using a Long Short-Term Memory neural network. The controller requires intraday point forecasts that are computed by an encoder-decoder architecture. Appendices VIII-A and VIII-B introduce the NFs and LSTM techniques implemented. Appendix VIII-D proposes a quality evaluation of the NFs and LSTM PV quantiles.

#### A. Normalizing Flows

We investigate the use of *Normalizing Flows* [16] that are a promising method for modeling stochastic generative processes. NFs define a new class of probabilistic generative models that has gained increasing interest from the deep learning community. They have proven to be an effective way to model complex data distributions with neural networks in many domains such as image, video, and audio generation [17], speech synthesis [18] or fundamental physics [19].

In this Appendix, let  $x$  be the random variable of interest, *i.e.*, the PV generation. Normalizing Flows, such as depicted in Figure 7, are defined as a sequence of invertible transformations  $f_k : \mathbb{R}^T \rightarrow \mathbb{R}^T$ ,  $k = 1, \dots, K$ , composed together to create an expressive invertible mapping  $f_\psi := f_1 \circ \dots \circ f_K : \mathbb{R}^T \rightarrow \mathbb{R}^T$ . This composed function can be used to perform density estimation, using  $f_\psi$  to map a sample  $\mathbf{x} \in \mathbb{R}^T$  onto a latent vector  $\mathbf{z} \in \mathbb{R}^T$  equipped with a known and tractable probability density function  $p_z$ , *e.g.*, a *Normal* distribution. The transformation  $f_\psi$  implicitly defines a density  $p_\psi(\mathbf{x})$  that is given by the change of variables

$$p_\psi(\mathbf{x}) = p_z(f_\psi(\mathbf{x})) |\det J_{f_\psi}(\mathbf{x})|, \quad (24)$$

where  $J_{f_\psi}$  is the Jacobian of  $f_\psi$  regarding  $\mathbf{x}$ . The model is trained by maximizing the log-likelihood  $\sum_{i=1}^N \log p_\psi(\mathbf{x}^i)$  of

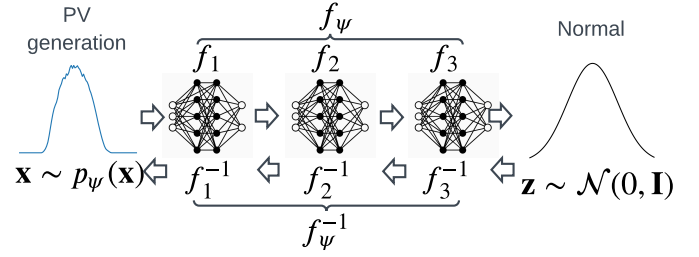


Fig. 7: A three-step NFs.

the model's parameters  $\psi$  given the dataset  $\mathcal{D}$ . The motivations to use NFs over more traditional deep learning approaches are three-fold:

- 1) Evaluating NFs in power system applications in terms of forecast value, and more particularly in the capacity firming framework. To the best of our knowledge, only [20] used NFs for the generation of daily load profiles. However, the model did not take into account the weather forecasts and the assessment is only performed on the forecast quality. In contrast, we implement a conditional NFs to compute improved weather-based PV forecasts.
- 2) NFs are capable of challenging state-of-the-art deep learning techniques in terms of quality, as demonstrated by [20]. Our study demonstrates they are also more accurate in terms of forecast value, and can be used effectively by non-expert deep learning practitioners.
- 3) NFs can directly be trained by maximum likelihood estimation. Therefore, in contrast to other deep learning generative models, *e.g.*, Generative Adversarial Networks (GANs) or Variational AutoEncoders (VAEs), NFs provide access to the exact likelihood of the model's parameters.

There are many possible implementations of NFs, see [17] for a comprehensive review. In this paper, the class of Affine Autoregressive flows is implemented<sup>5</sup>. A five-step Affine Autoregressive flow is trained by maximum likelihood estimation with 500 epochs, and a learning rate set to  $10^{-4}$ .

#### B. Long Short Term Memory

The NFs probabilistic day-ahead forecasts are compared to one of the most famous deep learning techniques adopted in energy forecasting applications: a Long Short-Term Memory neural network. More particularly the neural network implemented is composed of a LSTM cell and feed-forward layers, and is referred to as LSTM in the rest of the paper. The number of LSTM units is  $n_{\text{input}} + (n_{\text{output}} - n_{\text{input}})/3$ , and the number of neurons of the feed-forward layer  $n_{\text{input}} + 2 \times (n_{\text{output}} - n_{\text{input}})/3$ , with  $n_{\text{input}}$  and  $n_{\text{output}}$  the number of neurons of the input and output layers, respectively. The activation functions are the ReLU, the learning rate is set to  $10^{-3}$ , the number of epoch to 500 with a batch size of 64. The model is trained by quantile regression that consists of minimizing the quantile loss over the dataset.

<sup>5</sup><https://github.com/AWehenkel/Normalizing-Flows> [21]

### C. Encoder-Decoder

The intraday point forecasts are computed by an innovative architecture, referred to as encoder-decoder [10]. It is composed of two different networks and has recently shown promising results for translation tasks and speech recognition applications and imbalance price forecasting. The encoder-decoder processes features from the past, such as past PV observations, to extract the relevant historical information that is contained into a reduced vector of fixed dimensions, based on the last hidden state. Then, the decoder processes this representation along with the known future information such as weather forecasts. A version of the encoder-decoder architecture is implemented with a LSTM as the encoder and a multilayer perceptron as the decoder. The encoder has  $2 \times n_{\text{input}}$  units with  $n_{\text{input}}$  the number of neurons of the encoder input layer, features from the past. Then, the encoder output is merged with the weather forecasts becoming the decoder input layer that has  $n_{\text{output}}/2$  neurons. The activation functions are the ReLU, the learning rate is set to  $10^{-3}$ , and the number of epoch to 500 with a batch size of 64. The model is trained by minimizing the mean squared error over the dataset.

### D. Quantile forecasts quality evaluation

The *quantile score*, *reliability diagram*, and *continuous rank probabilistic score* are used to assess the quantile forecast quality of both the NFs and LSTM models. Forecast quality corresponds to the ability of the forecasts to genuinely inform of future events by mimicking the characteristics of the processes involved. Forecast value relates, instead, to the benefits from using forecasts in a decision-making process such as participation in the electricity market. In this Appendix, we focus only on the forecast quality evaluation.

Both NFs and LSTM models use the weather forecasts of the MAR (Regional Atmosphere Model) climate regional model provided by the Laboratory of Climatology of the Liège University [22]. The NFs model generates day-ahead scenarios, and the quantiles are derived. The LSTM model computes directly the quantiles as it is trained by minimizing the quantile loss. The set of PV quantiles considered for the assessment is  $\mathcal{Q} = \{q = 10\%, \dots, 90\%\}$ .

The continuous rank probability score (CRPS) [23] penalizes the lack of resolution of the predictive distributions as well as biased forecasts. It is negatively oriented, *i.e.*, the lower, the better, and for point forecasts, it turns out to be the mean absolute error. Let  $\hat{p}_{t+k|t}^q$  be the PV quantile forecast  $q$  generated at time  $t$  for lead time  $t+k$ . The energy form of the CRPS for lead time  $k$  is estimated following [24] over the dataset  $\mathcal{D}$  of length  $N \forall k = k_1, \dots, k_T$  as follows

$$\begin{aligned} \text{CRPS}(k) = & \frac{1}{N} \sum_{t \in \mathcal{D}} \left[ \frac{1}{Q} \sum_{q=1}^Q |\hat{p}_{t+k|t}^q - p_{t+k}| \right. \\ & \left. - \frac{1}{2Q^2} \sum_{q,q'=1}^Q |\hat{p}_{t+k|t}^q - \hat{p}_{t+k|t}^{q'}| \right]. \end{aligned} \quad (25)$$

The quantile score (QS) is complementary to the CRPS as it permits obtaining detailed information about the forecast

quality at specific probability levels, *i.e.*, over-forecasting or under-forecasting, and particularly those related to the tails of the predictive distribution [25]. It is negatively oriented and assigns asymmetric weights to negative and positive errors for each quantile. The quantile score for quantile  $q$  is estimated over the dataset  $\mathcal{D}$  of length  $N$  and for all lead times  $k$  as follows

$$QS(q) = \frac{1}{N} \sum_{t \in \mathcal{D}} \frac{1}{T} \sum_{k=k_1}^{k_T} \rho_q(\hat{p}_{t+k|t}^q, p_{t+k}), \quad (26a)$$

$$\rho_q(\hat{p}, p) := \max \{ (1-q)(\hat{p} - p), q(p - \hat{p}) \}. \quad (26b)$$

Finally, the reliability diagram is a graphical verification used to evaluate the reliability of the quantiles derived from the scenarios. Quantile forecasts are reliable if their nominal proportions are equal to the proportions of the observed value.

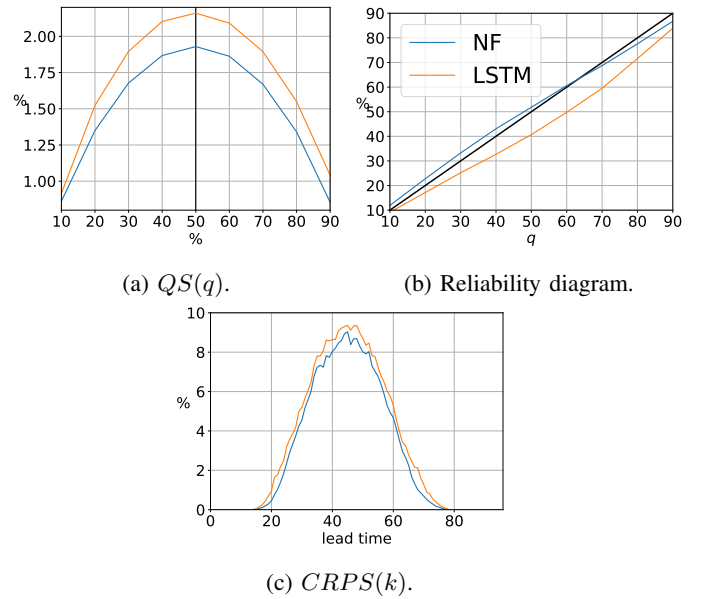


Fig. 8: Quantile forecast quality evaluation.

Figure 8 provides the results for these quality metrics computed over the entire dataset normalized by the total installed capacity. The NFs model outperforms the LSTM model with average values of 1.49 % and 2.80 % vs. 1.69 % and 3.15 % for the QS and CRPS, respectively. The NFs quantiles are also more reliable as indicated by the reliability diagram. These results motivate the use of the NFs as they outperform common deep learning approaches such as LSTM models. However, the core focus of this paper is robust optimization in the capacity framework. Therefore, an extensive NFs assessment in terms of forecast quality and value with a comparison with state-of-the-art deep learning models is out of the scope, and will be proposed in another study.